

PENGISIAN ACUAN DALAM PEMBUNGKUSAN ELEKTRONIK

(MOULD FILLING IN ELECTRONIC PACKAGING)

oleh

**CHU WEE LIANG
61163**

Penyelia

PROF. ASWASTHA NARAYANA

FEBRUARY 2004

**Disertai ini dikemukakan kepada
Universiti Sains Malaysia
Sebagai memenuhi sebahagian daripada syarat untuk
pengijazahan dengan kepujian**

SARJANA MUDA KEJURUTERAAN MEKANIK



**Pusat Pengajian Kejuruteraan Mekanik
Kampus Kejuruteraan
Universiti Sains Malaysia**

ACKNOWLEDGEMENT

I wish to take this opportunity to express my sense of gratitude to Prof. Aswatha Narayana for his guidance and moral support in my final year project. I am very lucky to be associated with him in pursuing my research interest.

Thanks to Mr. Tan Chun Wai, my mentor who is working in Intel now, for many constructive and useful suggestion and help to me in this final year project.

I am grateful to Mr. Glukaril for many fruitful discussions, encouragement and good wishes. I express my appreciation to Mr. Raju for his valuable suggestions.

Thanks also to all my fellow colleagues and friends for their support and help throughout the course of this work.

Lastly I would like to express my greatest thanks to my parents, because all I have accomplished in my life is granted by their unconditional love and years of sacrifice.

TABLE OF CONTENTS

ACKNOWLEDGEMENTS

i

TABLE OF CONTENTS

LIST OF FIGURES

LIST OF TABLES

NOMENCLATURE

ABSTRAK

ABSTRACT

CHAPTER 1 INTRODUCTION

- 1.1 Electronic packaging
- 1.2 What is encapsulation?
- 1.3 Encapsulation processes
 - 1.3.1 Molding
 - 1.3.2 Transfer molding process
- 1.4 Objective

CHAPTER 2 LITERATURE SURVEY

- 2.1 Introduction
- 2.2 Flow models in molding
- 2.3 Front tracking
- 2.4 Summary

CHAPTER3 APPROACHES FOR FLOW ANALYSIS

- 3.1 Two-dimensional Hele-Shaw approximation
 - 3.1.1 Finite element formulation
 - 3.1.1.1 Discretization of pressure equation
- 3.2 Pseudo-concentration approach
 - 3.6.1 Finite element formulation

CHAPTER 4 METHODOLOGY VERIFICATION

4.1 Newtonian flow

4.1.1 Filling a rectangular cavity

4.1.2 Filling a flat cavity in the xy-plane

4.2 Non-Newtonian flow

4.2.1 Hydraulic radius approximation for trapezoidal cross-section

4.2.2 Shape factor approximation for rectangular cross-section

4.2.3 Hele-Shaw approximation with rectangular cross-section

CHAPTER5 RESULTS AND DISCUSSIONS

5.1 Parametric Studies

5.1.1 Parametric Study for Newtonian flow

5.1.1.1 Parametric study for Gate's thickness

5.1.1.2 Parametric study for Gate's width

5.1.1.3 Parametric study for Gate's length

5.1.1.4 Parametric study for Runner's thickness

5.1.1.5 Parametric study for Runner's width

5.1.1.6 Parametric study for Vertical's velocity of the fluid, u

5.1.1.7 Parametric study for Viscosity of the fluid, η

5.1.2 Parametric Study for non-Newtonian flow

5.1.2.1 Parametric study for Gate's thickness

5.1.2.2 Parametric study for Gate's width

5.1.2.3 Parametric study for Gate's length

5.1.2.4 Parametric study for Runner's thickness

5.1.2.5 Parametric study for Runner's width

5.1.2.6 Parametric study for Vertical's velocity of the fluid, u

5.1.2.7 Parametric study for Material constant of the fluid, m_0

5.1.2.8 Parametric study for Power law indeks, n

5.2 Application of Parametric study in transfer molding simulation

5.2.1 Newtonian flow

5.2.1.1 Case 1

5.2.1.2 Case 2

5.2.1.3 Case 3

5.2.1.4 Case 4

5.2.1.5 Case 5

5.2.1.6 Case 6

5.2.1.7 Case 7

5.2.2 Non-Newtonian flow

5.2.2.1 Case 1

5.2.2.2 Case 2

5.2.2.3 Case 3

5.2.2.4 Case 4

5.2.2.5 Case 5

5.2.2.6 Case 6

5.2.2.7 Case 7

CHAPTER6 CONCLUSIONS

6.1 Transfer molding

6.1.1 Newtonian flow

6.1.2 Non-Newtonian flow

6.2 Future work

REFERENCES

APPENDIX

LIST OF FIGURES

Figure 1.1	Schematic of a transfer molding machine	1
Figure 1.2	Schematic of a transfer molding machine	
Figure 1.3	A typical transfer molding process	
Figure 3.1	The flow of polymer melt into a thin rectangular mold cavity	
Figure 4.1	A linear three-noded triangular element	
Figure 4.1	(a) Fluid filling a rectangular cavity (all dimension in mm) (b) Finite element mesh	
Figure 4.2	Velocity vectors plot across the rectangular cavity	
Figure 4.3	Comparison of front profiles between Gethin and Abdullah (1997) and present work	
Figure 4.4	Physical dimensions, boundary conditions for flow entering the cavity lying in the xy-plane (all dimension in mm)	
Figure 4.5	Finite element mesh	
Figure 4.6	Velocity vectors plot for flow in x-y plane cavity	
Figure 4.7	Comparison of front profiles between Gethin and Abdullah (1997) and present work	
Figure 4.8	Dimensions and boundary conditions for a rectangular runner	
Figure 4.9	(a) Cross sectional view of the runner used in the experiment (a) Cross sectional view of the model used in present work	
Figure 4.10	Finite element mesh	
Figure 5.1	Physical dimension and boundary conditions used in parametric study in transfer molding simulation.	

- Figure 5.2 Finite element mesh for parametric study.
- Figure 5.3 vectors plot for Gate's dimension (12mm in length, 1.8mm in thickness, 8mm in width) and Runner's dimension (36mm in length, 1.8mm in thickness, 6mm in width), Newtonian flow
- Figure 5.4 Front profiles. Gate's dimension (12mm in length, 1.8mm in thickness, 8mm in width) and Runner's dimension (36mm in length, 1.8mm in thickness, 6mm in width) , Newtonian flow
- Figure 5.5 Velocity vectors plot for Gate's dimension (12mm in length,1.6mm in thickness, 8mm in width) and Runner's dimension (36mm in length, 1.8mm in thickness, 6mm in width) , Newtonian flow
- Figure 5.6 Velocity vectors plot for Gate's dimension (12mm in length,2.0mm in thickness, 8mm in width) and Runner's dimension (36mm in length, 1.8mm in thickness, 6mm in width) , Newtonian flow
- Figure 5.7 Physical dimension and boundary conditions used in parametric study for Gate's width of transfer molding simulation.
- Figure 5.8 Finite element mesh for parametric study for gate's width. (a)8mm, (b)4mm and (c)12mm
- Figure 5.9 Velocity vectors plot for Gate's dimension (12mm in length,2.0mm in thickness, 4mm in width) and Runner's dimension (36mm in length, 1.8mm in thickness, 6mm in width) , Newtonian flow
- Figure 5.10 Velocity vectors plot for Gate's dimension (12mm in length,2.0mm in thickness, 12mm in width) and Runner's dimension (36mm in length, 1.8mm in thickness, 6mm in width) , Newtonian flow
- Figure 5.11 Physical dimension and boundary conditions used in parametric study for Gate's length of transfer molding simulation.
- Figure 5.12 Finite element mesh for parametric study for Gate's length. (a)12mm, (b)8mm and (c)16mm
- Figure 5.13 Velocity vectors plot for Gate's dimension (8mm in length,2.0mm

in thickness, 12mm in width) and Runner's dimension (36mm in length, 1.8mm in thickness, 6mm in width) , Newtonian flow

Figure 5.14 Velocity vectors plot for Gate's dimension (16mm in length,2.0mm in thickness, 12mm in width) and Runner's dimension (36mm in length, 1.8mm in thickness, 6mm in width) , Newtonian flow

Figure 5.15 Velocity vectors plot for Gate's dimension (16mm in length,2.0mm in thickness, 12mm in width) and Runner's dimension (36mm in length, 1.6mm in thickness, 6mm in width) , Newtonian flow

Figure 5.16 Velocity vectors plot for Gate's dimension (16mm in length,2.0mm in thickness, 12mm in width) and Runner's dimension (36mm in length, 2.0mm in thickness, 6mm in width) , Newtonian flow

Figure 5.17 Finite element mesh for parametric study for runner's width. (a)6mm, (b)4mm and (c)8mm.

Figure 5.18 Velocity vectors plot for Gate's dimension (16mm in length,2.0mm in thickness, 12mm in width) and Runner's dimension (36mm in length, 1.8mm in thickness, 4mm in width) , Newtonian flow

Figure 5.19 Velocity vectors plot for Gate's dimension (16mm in length,2.0mm in thickness, 12mm in width) and Runner's dimension (36mm in length, 1.8mm in thickness, 8mm in width) , Newtonian flow

Figure 5.20 Velocity vectors plot for Gate's dimension (16mm in length,1.8mm in thickness, 12mm in width) and Runner's dimension (36mm in length, 1.8mm in thickness, 8mm in width) , $u = 40\text{mm/s}$, Newtonian flow

Figure 5.21 Velocity vectors plot for Gate's dimension (16mm in length,1.8mm in thickness, 12mm in width) and Runner's dimension (36mm in length, 1.8mm in thickness, 8mm in width) , $u = 60\text{mm/s}$, Newtonian flow

Figure 5.22 Velocity vectors plot for Gate's dimension (16mm in length,1.8mm in thickness, 12mm in width) and Runner's dimension (36mm in length, 1.8mm in thickness, 8mm in width) , $\eta = 0.04\text{Pa}\cdot\text{s}$ Newtonian flow

- Figure 5.23 Velocity vectors plot for Gate's dimension (16mm in length, 1.8mm in thickness, 12mm in width) and Runner's dimension (36mm in length, 1.8mm in thickness, 8mm in width) , $\eta = 0.06\text{Pa}\cdot\text{s}$ Newtonian flow
- Figure 5.24 Velocity vectors plot for Gate's dimension (16mm in length, 1.8mm in thickness, 12mm in width) and Runner's dimension (36mm in length, 1.8mm in thickness, 8mm in width) , Non-Newtonian flow
- Figure 5.25 Front profiles. Gate's dimension (12mm in length, 1.8mm in thickness, 8mm in width) and Runner's dimension (36mm in length, 1.8mm in thickness, 6mm in width) , Non-Newtonian flow
- Figure 5.26 Velocity vectors plot for Gate's dimension (16mm in length, 1.6mm in thickness, 12mm in width) and Runner's dimension (36mm in length, 1.8mm in thickness, 8mm in width) , Non-Newtonian flow
- Figure 5.27 Velocity vectors plot for Gate's dimension (16mm in length, 2.0mm in thickness, 12mm in width) and Runner's dimension (36mm in length, 1.8mm in thickness, 8mm in width) , Non-Newtonian flow
- Figure 5.28 Velocity vectors plot for Gate's dimension (16mm in length, 1.8mm in thickness, 4mm in width) and Runner's dimension (36mm in length, 1.8mm in thickness, 8mm in width) , Non-Newtonian flow
- Figure 5.29 Velocity vectors plot for Gate's dimension (16mm in length, 1.8mm in thickness, 12mm in width) and Runner's dimension (36mm in length, 1.8mm in thickness, 8mm in width) , Non-Newtonian flow
- Figure 5.30 Velocity vectors plot for Gate's dimension (8mm in length, 1.8mm in thickness, 8mm in width) and Runner's dimension (36mm in length, 1.8mm in thickness, 8mm in width) , Non-Newtonian flow
- Figure 5.31 Velocity vectors plot for Gate's dimension (16mm in length, 1.8mm in thickness, 8mm in width) and Runner's dimension (36mm in length, 1.8mm in thickness, 8mm in width) , Non-Newtonian flow
- Figure 5.32 Velocity vectors plot for Gate's dimension (12mm in length, 1.8mm in thickness, 8mm in width) and Runner's dimension (36mm in length, 1.6mm in thickness, 8mm in width) , Non-Newtonian flow

- Figure 5.33 Velocity vectors plot for Gate's dimension (12mm in length, 1.8mm in thickness, 8mm in width) and Runner's dimension (36mm in length, 2.0mm in thickness, 8mm in width) , Non-Newtonian flow
- Figure 5.34 Velocity vectors plot for Gate's dimension (12mm in length, 1.8mm in thickness, 8mm in width) and Runner's dimension (36mm in length, 1.8mm in thickness, 4mm in width) , Non-Newtonian flow
- Figure 5.35 Velocity vectors plot for Gate's dimension (12mm in length, 1.8mm in thickness, 8mm in width) and Runner's dimension (36mm in length, 1.8mm in thickness, 8mm in width) , Non-Newtonian flow
- Figure 5.36 Velocity vectors plot for Gate's dimension (16mm in length, 1.8mm in thickness, 12mm in width) and Runner's dimension (36mm in length, 1.8mm in thickness, 8mm in width) , $u = 40\text{mm/s}$, Non-Newtonian flow
- Figure 5.37 Velocity vectors plot for Gate's dimension (16mm in length, 1.8mm in thickness, 12mm in width) and Runner's dimension (36mm in length, 1.8mm in thickness, 8mm in width) , $u = 60\text{mm/s}$, Non-Newtonian flow
- Figure 5.38 Velocity vectors plot for Gate's dimension (16mm in length, 1.8mm in thickness, 12mm in width) and Runner's dimension (36mm in length, 1.8mm in thickness, 8mm in width) , $m_0 = 0.000393\text{MPa}\cdot\text{s}^n$ Non-Newtonian flow
- Figure 5.39 Velocity vectors plot for Gate's dimension (16mm in length, 1.8mm in thickness, 12mm in width) and Runner's dimension (36mm in length, 1.8mm in thickness, 8mm in width) , $m_0 = 0.0011796\text{MPa}\cdot\text{s}^n$, Non-Newtonian flow
- Figure 5.40 Velocity vectors plot for Gate's dimension (16mm in length, 1.8mm in thickness, 12mm in width) and Runner's dimension (36mm in length, 1.8mm in thickness, 8mm in width) , $n = 0.70$ Non-Newtonian flow
- Figure 5.41 Velocity vectors plot for Gate's dimension (16mm in length, 1.8mm in thickness, 12mm in width) and Runner's dimension (36mm in length, 1.8mm in thickness, 8mm in width) , $n = 1.10$ Non-Newtonian flow

- Figure 5.42 Physical dimensions and boundary conditions used in Newtonian flow simulation of transfer molding.
- Figure 5.43 Finite element mesh. Uniform gate's dimension (12mm in length and 1.8mm in thickness) and runner's dimension (6mm in width and 1.8mm in thickness).
- Figure 5.44 Velocity vectors plot for uniform gates' dimension (12mm in length and 1.8 mm in thickness) and runner's dimension (6mm in width and 1.8mm in thickness).
- Figure 5.45 Front profiles. Uniform gates' dimension (12mm in length and 1.8mm in thickness) and runner's dimension (6mm in width and 1.8mm in thickness)
- Figure 5.46 Physical dimensions and boundary conditions used in Newtonian flow simulation of transfer molding, Runner's width = 8mm.
- Figure 5.47 Finite element mesh. Uniform gate's dimension (12mm in length and 1.8mm in thickness) runner's dimension (8mm in width and 1.8mm in thickness).
- Figure 5.48 Velocity vectors plot for uniform gates' dimension (12mm in length and 1.8 mm in thickness) and runner's dimension (8mm in width and 1.8mm in thickness).
- Figure 5.49 Front profiles. Uniform gates' dimension (12mm in length and 1.8mm in thickness) and runner's dimension (8mm in width and 1.8mm in thickness)
- Figure 5.50 Physical dimensions and boundary conditions used in Newtonian flow simulation of transfer molding, Runner's width = 10mm.
- Figure 5.51 Finite element mesh. Uniform gate's dimension (12mm in length and 1.8mm in thickness) runner's dimension (10mm in width and 1.8mm in thickness).
- Figure 5.52 Velocity vectors plot for uniform gates' dimension (12mm in length and 1.8 mm in thickness) and runner's dimension (10mm in width and 1.8mm in thickness).

- Figure 5.53 Front profiles. Uniform gates' dimension (12mm in length and 1.8mm in thickness) and runner's dimension (10mm in width and 1.8mm in thickness)
- Figure 5.54 Velocity vectors plot for uniform gates' dimension (12mm in length, thickness in proportion of 0.9mm: 1.2mm: 1.8mm) and runner's dimension (10mm in width and 1.8mm in thickness).
- Figure 5.55 Front profile: Uniform gates' dimension (12mm in length and thickness in proportion of 0.9mm: 1.2mm: 1.8mm) and runner's dimension (10mm in width and 1.8mm in thickness)
- Figure 5.56 Velocity vectors plot for uniform gates' dimension (12mm in length, thickness in proportion of 0.7mm: 1.2mm: 1.8mm) and runner's dimension (10mm in width and 1.8mm in thickness).
- Figure 5.57 Front profile: Uniform gates' dimension (12mm in length and thickness in proportion of 0.7mm: 1.2mm: 1.8mm) and runner's dimension (10mm in width and 1.8mm in thickness)
- Figure 5.58 Velocity vectors plot for uniform gates' dimension (12mm in length, thickness in proportion of 0.7mm: 0.9mm: 1.8mm) and runner's dimension (10mm in width and 1.8mm in thickness).
- Figure 5.59 Front profile: Uniform gates' dimension (12mm in length and thickness in proportion of 0.7mm: 0.9mm: 1.8mm) and runner's dimension (10mm in width and 1.8mm in thickness)
- Figure 5.60 Velocity vectors plot for uniform gates' dimension (12mm in length, thickness in proportion of 0.7mm: 0.9mm: 1.5mm) and runner's dimension (10mm in width and 1.8mm in thickness).
- Figure 5.61 Front profile: Uniform gates' dimension (12mm in length and thickness in proportion of 0.7mm: 0.9mm: 1.5mm) and runner's dimension (10mm in width and 1.8mm in thickness)
- Figure 5.62 Physical dimensions and boundary conditions used in Non-Newtonian flow simulation of transfer molding.
- Figure 5.63 Finite element mesh. Uniform gate's dimension (8mm in width

and, 1.8mm in thickness and length in proportion of 8mm: 12mm: 16mm) and runner's dimension (6mm in width and 1.8mm in thickness)

- Figure 5.64 Velocity vectors plot. Gate's dimension (8mm in width, 1.8mm in thickness and length in proportion of 8mm: 12mm : 16mm) and runner's dimension (6mm in width and 1.8mm in thickness).
- Figure 5.65 Front profiles. Gate's dimension (8mm in width, 1.8mm in thickness and length in proportion of 8mm: 12mm: 16mm) and runner's dimension (6mm in width, 1.8mm in thickness).
- Figure 5.66 Physical dimensions and boundary conditions used in Non-Newtonian flow simulation of transfer molding, Runner's width = 8 mm
- Figure 5.67 Finite element mesh. Uniform gate's dimension (8mm in width and, 1.8mm in thickness and length in proportion of 8mm: 12mm: 16mm) and runner's dimension (8mm in width and 1.8mm in thickness)
- Figure 5.68 Velocity vectors plot. Gate's dimension (8mm in width, 1.8mm in thickness and length in proportion of 8mm: 12mm : 16mm) and runner's dimension (8mm in width and 1.8mm in thickness).
- Figure 5.69 Front profiles. Gate's dimension (8mm in width, 1.8mm in thickness and length in proportion of 8mm: 12mm: 16mm) and runner's dimension (8mm in width, 1.8mm in thickness).
- Figure 5.70 Physical dimensions and boundary conditions used in Non-Newtonian flow simulation of transfer molding, Runner's width = 10 mm
- Figure 5.71 Finite element mesh. Uniform gate's dimension (8mm in width and, 1.8mm in thickness and length in proportion of 8mm: 12mm: 16mm) and runner's dimension (10mm in width and 1.8mm in thickness)
- Figure 5.72 Velocity vectors plot. Gate's dimension (8mm in width,

1.8mm in thickness and length in proportion of 8mm: 12mm : 16mm) and runner's dimension (10mm in width and 1.8mm in thickness).

Figure 5.73 Front profiles. Gate's dimension (8mm in width, 1.8mm in thickness and length in proportion of 8mm: 12mm: 16mm) and runner's dimension (10mm in width, 1.8mm in thickness).

Figure 5.74 Velocity vectors plot for uniform gates' dimension (8mm in width, 1.8mm in thickness and length in proportion of 8mm : 12mm: 16mm) and runner's dimension (10mm in width and 2.0mm in thickness).

Figure 5.75 Front profile for uniform gates' dimension (8mm in width, 1.8mm in thickness and length in proportion of 8mm : 12mm: 16mm) and runner's dimension (10mm in width and 2.0mm in thickness).

Figure 5.76 Velocity vectors plot for uniform gates' dimension (8mm in width, thickness in proportion of 0.8:0.9:1.8 and length in proportion of 8mm: 12mm: 16mm) and runner's dimension (10mm in width and 2.0mm in thickness).

Figure 5.77 Front profiles. Uniform gates' dimension (8mm in width, thickness in proportion of 0.8:0.9:1.8 and length in proportion of 8mm: 12mm: 16mm) and runner's dimension (10mm in width and 2.0mm in thickness).

Figure 5.78 Velocity vectors plot for uniform gates' dimension (8mm in width, thickness in proportion of 0.9:0.9:1.8 and length in proportion of 8mm: 12mm: 16mm) and runner's dimension (10mm in width and 2.0mm in thickness).

Figure 5.79 Front profiles. Uniform gates' dimension (8mm in width, thickness in proportion of 0.9:0.9:1.8 and length in proportion of 8mm: 12mm: 16mm) and runner's dimension (10mm in width and 2.0mm in thickness).

Figure 5.80 Velocity vectors plot for uniform gates' dimension (8mm in width, thickness in proportion of 0.9:1.0:1.8 and length in proportion of 8mm: 12mm: 16mm) and runner's dimension

(10mm in width and 2.0mm in thickness).

- Figure 5.81 Front profiles. Uniform gates' dimension (8mm in width, thickness in proportion of 0.9:1.0:1.8 and length in proportion of 8mm: 12mm: 16mm) and runner's dimension (10mm in width and 2.0mm in thickness).
- Figure A1 The shape factor for flow of a power law fluid in a rectangular cross-section channel (Middleman, 1997)
- Figure A2 drop data for flow of an epoxy molding compound in a trapezoidal cross-section runner. The flow length was 26 cm. The flow was non-isothermal and the material was heating as it flowed. (Manziona, 1990)

LIST OF TABLE

- Table 4.1 Comparison of pressure drop values obtained from different approaches
- Table 5.1 Results of parametric study for gate's thickness, Newtonian flow.
- Table 5.2 Results of parametric study for gate's width, Newtonian flow
- Table 5.3 Results of parametric study for gate's length, Newtonian flow
- Table 5.4 Results of parametric study for runner's thickness, Newtonian flow
- Table 5.5 Results of parametric study for runner's width, Newtonian flow
- Table 5.6 Results of parametric study for flow' horizontal velocity, u , Newtonian flow
- Table 5.7 Results of parametric study for flow' viscosity, η , Newtonian flow
- Table 5.8 Results of parametric study for gate's thickness, Non-Newtonian flow
- Table 5.9 Table 5.9 Results of parametric study for gate's width, Non-Newtonian flow

Table 5.10	Table 5.10 Results of parametric study for gate's length, Non-Newtonian flow
Table 5.11	Results of parametric study for runner's thickness, Non-Newtonian flow
Table 5.12	Results of parametric study for runner's width, Non-Newtonian flow
Table 5.13	Results of parametric study for flow' horizontal velocity, u, Non-Newtonian flow
Table 5.14	Results of parametric study for material constant, Non-Newtonian flow
Table 5.15	Results of parametric study for flow's power law index

NOMENCLATURE

Symbols

A	Area
a_f	Flow area
2b	Cavity thickness
[B]	Gradient matrix
[D]	Material property matrix
F	Pseudo-concentration
{f}	Loading vector
IC	Integrated circuit
k	Thermal conductivity
[K]	Stiffness matrix

L	Length
m_o	Material constant
N	Power law index
N_i, N_j, N_k	Shape function
S	Fluidity
T	Thickness/ time
\bar{u}	Volume averaged velocity in x-direction
\bar{v}	Volume averaged velocity in y-direction
ρ	Density
ν_{ad}	Artificial diffusivity
μ, η	Viscosity
γ	Shear rate
Ω	Domain

ALIRAN ACUAN DALAM PEMBUNGKUSAN ELEKTRONIK

ABSTRAK

Projek tahun akhir ini tertumpu kepada kajian ke atas aliran bendalir dalam proses enkapsulasi yang khas digunakan dalam industri pembungkusan elektronik. Model Hele-Shaw 2D digunakan adalah untuk meninjau sifat-sifat aliran bendalir Newtonian dan bukan Newtonian (power law) ke dalam rongga-rongga yang tertabur pada jarak yang berlainan dari ram permindahan dalam proses pengacuanan permindahan. Taburan halaju bendalir diperoleh daripada kaedah Hele-Shaw digunakan dalam algoritma pseudo-kepekatan untuk mengesan muka hadapan bendalir dengan penambahan ungkapan artificial diffusion. Fungsi ungkapan artificial diffusion ialah membenarkan gelinciran separa, di permukaan bendalir-dinding dan memadamkan ayunan berangka (numerical oscillation) ke tahap minimum. Kaedah berangka tak terhingga digunakan dalam analisis untuk menurunkan persamaan-persamaan pemerintah pembezaan separa kepada persamaan-persamaan algebra. Kajian parameter telah dijalankan untuk meninjau bagaimana parameter-parameter atau dimensi-dimensi acuan mempengaruhi sifat-sifat aliran bendalir dalam acuan. Hasil daripada kajian parameter kita seterusnya dapat menunjukkan rintangan hidraulik yang dikenakan ke atas bendalir yang diagihkan ke dalam rongga-rongga sesiri dalam pengacuan permindahan boleh ditentukan pada nisbah yang sesuai supaya mencapai pengisian seimbang dengan hanya mengubah dimensi-dimensi acuan pada nisbah luas keratan rentas yang sesuai.

ABSTRACT

This final year project focuses on the study of flow in encapsulation processes in electronic packaging industry. The present work adopted a 2D Hele-Shaw model to study the flow of Newtonian and Non-Newtonian (power law) fluids into cavities at various distances from transfer ram in the transfer molding process. The velocity field obtained from both Hele-Shaw and generalized porous medium approaches is used in pseudo-concentration algorithm for front tracking with an artificial diffusion term added to allow partial slip at the fluid-wall interface and to damp numerical oscillation to a minimum level. Finite Element Method is employed in all the analyses to reduce the governing partial differential equations to algebraic equations. Parametric studies had been carried out to study how the dimension and parameter of the mold tools affects the flow filling's behavior. From parametric study we can show that by altering the dimensions of mold tools, thus introducing different hydraulic resistances at various in-line cavities in appropriate proportions, will lead to balance filling in transfer molding.

Chapter 1

INTRODUCTION

1.1 Electronic packaging

The electronic packaging design performs tasks of ever increasing importance in the electronic industry. Electronic packaging often benefits from technologies developed for the encapsulation of integrated circuits (ICs). The key functions of an electronic package are to protect, power and cool the microelectronic chips or components and provide electrical and mechanical connection between the microelectronic parts and the outside world. The challenge for the package is to provide all crucial functions required by the electronic parts without limiting the performance. As the semiconductor technology progresses towards higher levels of integration, high performance and increasing functionality, the design and fabrication of the package that will meet the modern requirements and future microelectronic systems becomes increasingly complex and challenging.

The package is already the bottleneck to the system performance, as demonstrated for the maximum digital system clock frequencies shown in figure 1. 1. The clock frequency on the IC is higher than that possible for the package. It is evident the package limits the IC technology. The simple fact is that the on-chip silicon system can out-perform the speed capability of the package. Furthermore, as volume production techniques continue to drive the cost of bare chips down, the cost of the packaging constitutes a greater and greater portion of the total system cost. Hence, the challenges for future electronic packages are becoming extremely complex and many aspects that will likely affect the performance of an electronic package must be considered thoroughly. Tremendous research efforts have to be committed to come out with an optimum packaging design.

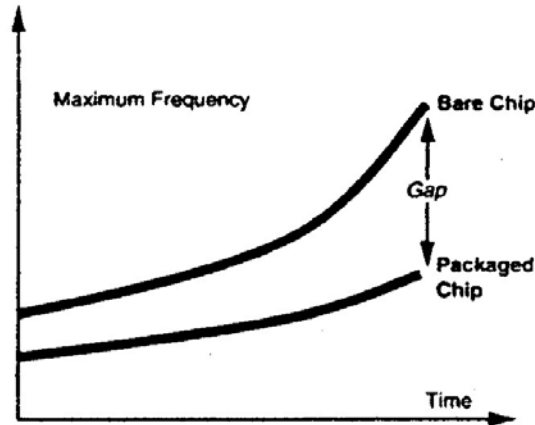


Figure 1.1: IC packaging performance gap (Tummala, 2001)

1.2 What is encapsulation?

An electronic device cannot perform its designed function until it is packaged such that it is interconnected with the rest of the system and protected. One such protection technology that has been commonly used is encapsulation, is done typically by means of low temperature polymers. Encapsulation provides an economical way to protect device packages by isolating the active devices from environmental pollutants, and at the same time offering mechanical protection by structural coupling of the device to the constituent packaging materials into a robust package.

Encapsulation materials are typically molded onto the IC or dispensed under the die, such as with flip chip BGA packages. This type of organic coating is a very inexpensive way of protecting devices, but their protection is not permanent. Typically controlled by permeation properties of the polymeric resin used. The inorganic sealing however, is permanent, by being hermetic, but the cost of this process is high.

Inadequate adhesion, contaminants within the raw material, incompatible thermal expansion, and stress-related problems, in addition to a relatively immature knowledge of filler technology to control the CTE (Coefficient of Thermal Expansion) mismatch, all combined to account for the delayed acceptance of non-hermetic plastic packages. With significant efforts in the areas of resins, fillers, material formulations, and process

development work, polymer packaging finally began to make its presence felt in the early 1980s. Semiconductor International, 1987, reported plastic packages account for approximately 80 % of the worldwide package share and this percentage has been increasing.

Significant progress was made in improving the quality of the glass passivation layer that is deposited on the active areas of the device, as a first line of defence against moisture-related problems. The combination of these technological advances provided the essential increase in reliability that was needed for polymeric packaging to begin in today's widespread use. It is believed that the polymeric packages will continue to grow their share in the device encapsulation area, and one day hermetic packages may become a custom-made item, only for those interested in applications in unusual environments such as in space and deep sea.

Performance of encapsulation is determined by its dimensional-stability, its resistance to thermal excursions, its permeation providing isolation of environmental pollutants and its thermal dissipation providing dissipation of heat generated by the packaged device. The progress in encapsulation technology during last two decades has allowed plastic-encapsulated microcircuits to be used in some of the most demanding applications, including space-borne electronic systems, as a cost-effective device protection. (Tummala, 2001).

1.3 Encapsulation processes

Encapsulation process can be classified into two major categories: molding and liquid encapsulation.

1.3.1 Molding

The majority of encapsulating processes in the IC packaging market are transfer molding. By applying pressure, the heated molten molding compound is transferred from a pot

(plunger), through the runners, and into the mold cavities. This is a simple mass production and low-cost method for most device encapsulation. However, the transfer molding method is hard to apply to some new applications such as flip chip and cavity fill type PGA (pin-grid array). Molding operation can be done individually on a single device or in molded array packages (MAP). The latter requires careful design of the mold so that defects, such as wire sweep and void entrapment, are minimized to a single device molding level. Spherical silica fillers used in the molding compounds for the MAP operation also help to minimize defects.

1.3.2 Transfer molding process

A transfer mold contains a series of in-line cavities, one for each eventual semiconductor package. Each cavity has very small exhaust channels, called vents, which allow air to exit the cavity as the molding compound enters. A runner is laid parallel to the strip cavity set, and it feeds the molding compound to each cavity through small entrance pots called gates. Usually, the runners are cut into only one half of the mold. Large molds also contain primary runners, which connect these strip runners to the main transfer pot. The transfer pot is a cylinder cut through one of the mold halves, and it receives the molding compound initially. It is often near the center of the mold. Knockout pins lay flush with the runner and cavity surface during the molding cycle and then extend into those regions to push the molded devices and runners out when the mold opens. The mold may contain heater elements within its body, or it may depend on heat transfer from the press structure.

The operational process is simple and usually automated: The mold opens and new strip of several in-line, pre-assembled devices, loaded into the in-line cavities. The actual active silicon devices are somewhere near the middle of the cavities. The mold closes and the molding compound, almost always a solid tablet, is placed into the transfer pot. This tablet may be pre-heated, or it may rely on heat transfer from the mold. Then the transfer ram compresses the tablet into runner systems. By the time material starts to enter the cavities, it is fully molten and usually at its viscosity minimum. The pressure then increases to about 6.4 MPa to "pack-out" the molding compound. This increase in pressure effectively reduces

the diameters of any voids to fourth of their original values, and it ensures that the sharp cavity corners fill out completely. This pressure holds until the molding compound cures, and becomes rigid enough to support the devices and the strips. The mold opens, the knockout pins automatically extend, and all molded gates and runners eject into collection systems. Brushes then clean away any residue or "flash" molding compound, and the cycle begins again.

“Conventional” molds dominated in the 1970s through the 1980s. These were huge, complex mold with a single, large pot often holding up to a half-kilogram EMC (Epoxy Molding Compound) tablet. There were several dozens to a thousand individual package cavities. The strip loading, tablet loading, parts removal and cleaning operations were usually manual because of the complexity of the molds. While these molds were extremely economical, they were also "unbalanced", meaning that some cavities were filled sooner than others. This design allowed variations in gold interconnection wire movement (called "wire sweep"), and variations in void level and sizes. Cycle times usually varies from 90 to 240 seconds.

Newer molds now used several smaller pots and rams and the cavities are symmetrically located. These are balanced and all cavities experience the same flow profiles and pressure profiles during fill. These are called gang-pot molds because of the chain-gang alignment of the plungers and pots.

The presses, which hold and operate the mold, have three main functions: they clamp the molds closed, they move the transfer ram and they control the mold temperature. Automated presses, typical for gang-pot molds, manage all other functions like device loading, device/ runner ejection and cleaning robotically with almost no operator input. Hydraulic clamping and transfer control is tending towards stepping motor control. Cycle times under a minute are typical and some operate as low as 15 seconds. A state-of-the-art auto, gang-pot press cost at least several hundred thousand dollars. Figure 1.2 shows schematic of a transfer molding machine -and figure 1.3 depicts the typical molding process. (Tummala, 2001).

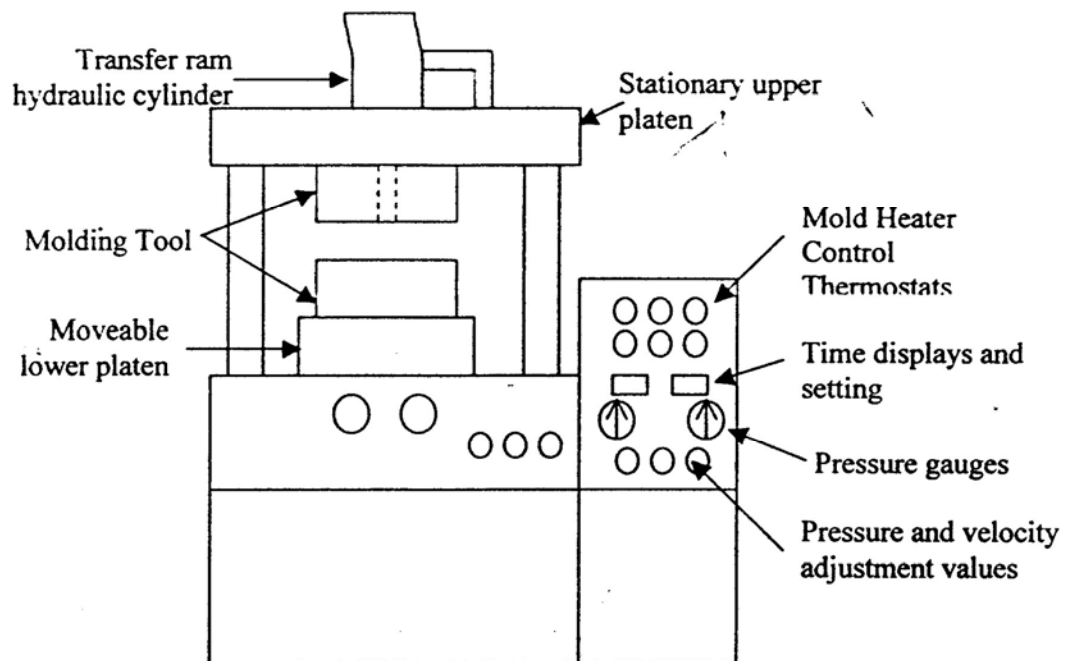


Figure 1.2: Schematic of a transfer molding machine (Manziona, 1990)

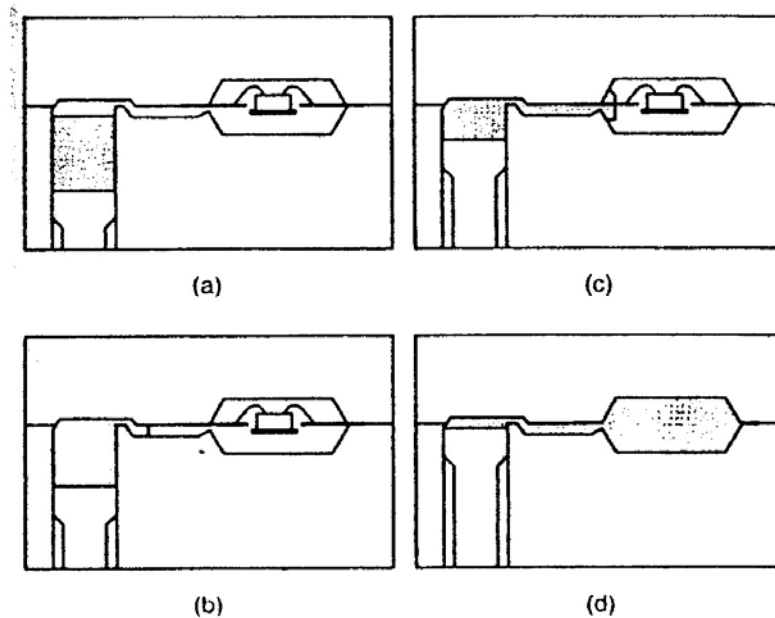


Figure 1.3: A typical transfer molding process (Tummala, 2001)

1.4 Objective

The objectives of the present work are listed below:

- Establish a general solution algorithm to model the flow of fluids (Newtonian and Non-Newtonian) in transfer molding.
- Conduct parametric studies using Finite Element code developed. The results can be further utilized as a design guideline to optimize the encapsulation process prior to fixing of actual manufacturing setup.
- Illustrate an application of parametric studies made for a practical mold tools configuration for both Newtonian and Non-Newtonian fluids.

Chapter 2

LITERATURE SURVEY

2.1 Introduction

Plastic ICs encapsulation provides an economical and efficient way to package an IC in order to protect and enable the optimal performance of an electronic package. Basically, encapsulation can be classified into two major categories: molding and liquid encapsulation (Tummala, 2001). Intensive research efforts have been carried out in flow simulation of low temperature polymers (molding compounds) used in encapsulation for various package designs ranging from wire bonding, chip carrier with beam leads to direct chip connection (Gilleo, 2001).

Transfer molding of ICs is a well-established step in the manufacture of plastic packages. Although it is a mature technology, transfer molding is still difficult to optimize and remains subject to several manufacturing defects, including incomplete encapsulation, void formation and excessive deformation of wires and leadframes (Nguyen et al., 2000). Recent advances in other areas of packaging, namely fine pitch wirebonding (Nguyen et al., 1998) and molded array package technologies, have increased the risk of defects, and imposed even more demanding requirements on the molding process (Nguyen and Lee, 1998) and on the material formulation (Nguyen et al., 1997). For better mold design and optimization of processing, flow analysis during the encapsulation process is needed.

2.2 Flow models in molding

Most of the researchers modeled flow of Newtonian and non-Newtonian fluid in a thin section, which resembles a mold cavity for plastic encapsulation, using Hele-Shaw approximation. The assumptions of using Hele-Shaw approximation are as follows:

- thickness of the model is relatively small as compared to its width and length
- viscous effect dominates the flow, thus inertia effect is negligible
- the fluid is generalized as Newtonian

The idea of using finite elements for simulating the filling of arbitrary molds was introduced by Hieber and Shen (1980), who generalized the Hele-Shaw flow approach to the use of generalized Newtonian fluids; the model was later extended by Hieber and Shen (1983) to the case of molds of variable thickness.

A method to simplify the treatment of flow analysis in a thin cavity with a group of inserts regularly-aligned for injection molding process is presented by Zhang and Zheng (1995). For a cavity without inserts or only with a few individual inserts, with the known temperature distribution in the fluid melt and melt properties, the flow conductance, S can be calculated with pressure gradient distribution. Of course iteration is needed to reevaluate the pressure gradient from the resulting pressure distribution.

Holm and Langtangen (1999) presented a simulation model for injection molding. A 2-dimensional Hele-Shaw approximation is adopted for the polymer flow between two flat plates, whereas the moving polymer-air front is handled by a level-set-like method. The 3-dimensional heat equation is solved using finite differences in time domain. The main advantage of the model is that a common 2-dimensional finite element mesh can be used for all the equations.

Chen et al. (1998) developed a numerical algorithm to simulate the filling stage of injection compression molding (ICM) process. Hele-Shaw fluid flow model combined with the control volume / finite element (CV/FEM) method is implemented to predict the melt front advancement and the distributions of pressure, temperature and flow velocity dynamically during melt filling process. The simulated molding pressures were also compared with those obtained by conventional injection molding (CIM). The simulated pressures for both ICM and CIM show good coincidence with those obtained from the cavity pressure measurements. Liu et al. (1996) coded a typical resin transfer molding encompasses of four

phases which are preform manufacturing, mold filling, resin curing and demolding. Filling phase is the core of the process. In their work, Hele Shaw approximation has been employed to analyze the resin flow. Finite Element Method was adopted for pressure calculation and control volume approach with a series of pseudo-steady states as for low Reynolds number flows, was used to compute the moving boundary. This work presents three simulation features developed in an existing mold filling simulation code, LIMS (Liquid Injection Molding Simulation), for resin transfer molding to address the processing issues of gate control, venting, and dry spot formation. The prevention of dry spots can be achieved by controlling the gate opening, hence changing the flow rate of resin fed into the cavity. The gates are controlled according to the filling status at the location in the mold where sensors are placed. Once the flow front reaches a sensor, the sensor will send a signal to control injection gates by opening or closing the valves or adjusting the pressure or flow rates.

In the study by Turng and Wang (1993) and Nguyen (1994), a finite element method based on the Hele-Shaw approximation has been used. The behavior of the epoxy molding compound is described by a generalized Newtonian fluid model. Although the geometry in the chip cavity is complicated, analysis is carried out for a simplified geometry by treating the leadframe as a solid.

Hang and Wang (2000) used Hele-Shaw approximation to analyze the flow in the chip cavity, particularly flow through the openings in the leadframes. Two methods to model cross flow through the openings in the leadframe have been proposed. In the first method, the flow through the leadframe opening has been modeled as a source term in the continuity equation. The value of the source term in the continuity equation was calculated using analytical equations for the pressure drop during flow through openings. In the second method, the cross flow has been modeled using a cross-flow element that connects the lower and upper chip cavity. The thickness of the cross-flow element is determined using analytical equations for the pressure drop during flow through openings. It is reported that both methods gave similar results but the first method is suitable for package with many small openings in the leadframe.

The plastic encapsulation process for a 144-lead TQFP package was studied both experimentally and computationally by Nguyen (2000). The computational models are constructed from 3-dimensional structured grid. The experimental results are obtained using an instrumented molding press. Short shot is performed at different instants before the cavity is filled. The computational simulation predictions are obtained by using software, namely PLICE-CAD. Both sets of results were in good agreement. It was also found that at normal and high fill rates, there is insufficient time for the resin conversion to greatly affect the viscosity of the commercial transfer molding compound. The authors also clearly explained the effects of fluid viscosity with respect to temperature and chemical conversion rate. The increasing temperature and conversion have opposite effects on the viscosity. Increased temperature reduced the viscosity, while the increased conversion raised the viscosity. The net effect is a slight reduction in the viscosity of the mold compound underneath and above the die as shown in the simulation. It is also stated that viscosity change due to temperature change are virtually instantaneous, but viscosity changes due to conversion are slower at intermediate process temperature. The kinetics required a finite length of time at a given temperature before the conversion increases, thus the viscosity conversion will initially lag the temperature-induced viscosity reduction. If the process occurs rapidly, there will be insufficient time for the conversion to significantly affect the viscosity.

Isothermal flow simulation of liquid composite molding has been carried out by Liu (2000) adopting finite element/nodal volume (FE/NV) procedure using Darcy's law to model the resin flow through the fibrous reinforcement. In the study, the effects of temperature and curing kinetics of the resin were ignored. This can be a reasonable assumption for the injection stage of Resin Transfer Molding process as the resin is usually injected fairly fast and the filling time is much less than the curing time.

Studies have been carried out by Kuah (1999) using commercial software C-MOLD with a view to design the gate and runner systems such that a balance flow achieved, thus minimizing wire sweep during the encapsulation of the QFP IOOL ultra fine pitch wire bonded package. The software models the mold filling by assuming a Hele-Shaw flow of

an incompressible viscous polymeric melt under non-isothermal and symmetric thermal boundary conditions. The numerical scheme is a hybrid finite element/finite difference method which solves pressure and temperature fields. The moving melt fronts are tracked by a control volume method. The numerical results have been compared to actual short shot sample and the results are compared well.

Some of the critical aspects addressed with short-shot experimentation are stated as follows (Kuah, 1999):

- Jetting - when the molding compound enters the mold cavity in a jet form, usually leading to a degradation in the wire bond quality
- Spiking - a sudden increase in mold compound velocity toward the end of the filling phase, leading to severe wire sweep
- Racing - a difference in the velocity of mold compound in the upper and lower halves of the mold, usually resulting in die tilt and deformed loops

Bickerton (1999) has investigated the effect of race tracking using equivalent permeability approach. Air channel can be presented within a mold cavity, either unintentionally formed or intentionally placed to enhance the mold filling process. Such channels provided paths of relatively low flow resistance, and can drastically alter flow front advancement and injection pressure, namely race tracking. The equivalent permeability magnitudes were based upon steady-state, fully developed flow through a rectangular duct.

2.3 Front tracking

The primitive variables, i.e. velocity and pressure fields, obtained from flow analysis have to be coupled with front tracking algorithm making the advancement of fluid in a cavity traceable at any instant before the cavity is filled.

When modeling the free surface, consideration may be given either the VOF (Volume of Fluid) method or the Lagrangian method (Hirt et al., 1974). The latter approach has an advantage since it naturally gives the position of the free surface via its moving boundary as the fluid fill the cavity. However, as the mesh keeps changing in size and position, a robust unstructured automatic mesh generator is required since frequent remeshing is needed owing to rapid distortion and movement of the free surface. Hence, it is more economical to use the Eulerian approach, which only requires a fixed mesh, and therefore the VOF method has been adopted for free surface tracking. Generally the algorithm for tracking free surface, based on volume of fluid (VOF) method, has been introduced by Hirt and Nichols (1995). This method has been used in conjunction with the continuity and Navier-Stoke equations by many authors in the literature to solve mold filling problems.

Gethin and Abdullah (1997) did a finite element formulation for filling thin sections. The formulation is based on an analogy that the local velocity profile across the thin section mimics the laminar Poiseuille flow between two surfaces. The velocity and the pressure fields were coupled with the VOF method to predict the free surface. The VOF method is written in the form of a first-order pure advection equation forming pseudo-concentration equation.

Prasad (1999) has used a front tracking technique namely Pseudo-concentration method with an additional artificial diffusion term. The functions of the artificial diffusion are to allow partial slip at polymer-wall interface and to damp numerical oscillation in the algorithm. This technique is based on the volume of fluid method (VOF), employs a well-known marker and cell (MAC) technique. A particular value of the pseudo-concentration variable, F was chosen to represent the free surface demarcating the polymer and air regions, which can be tracked for each time step. The main advantage of this method is that the location for the moving front and the front boundary conditions need not be explicitly accounted for.

Among the numerous numerical procedures developed, a class of the so called finite element/control volume (FE/CV) methods (Chen et al., 1998, Liu, 1996 and Kuah, 1999)

have been gaining popularity due to their simplicity and efficiency in dealing with the flow simulation. In these methods, a fixed finite element mesh is used for the entire domain to be simulated. The 3 basic steps in FE/CV methods are (1) obtain the pressure distribution in the resin-filled region, (2) calculate the resin flow rates; and (3) trace the resin flow front. Out of these 3 steps, the first step requires the use of finite element solution. (Joshi et al., 2000).

The drawback of FE/CV method was construction of control volumes for the flow calculation based on the finite element mesh. This could be time consuming and complex for large parts with complicated geometry. Liu (2000) proposed a finite element/nodal volume (FE/NV) procedure for the isothermal flow simulation of liquid composite molding processes. This method does not require the construction of control volumes explicitly. In addition, no special treatment is needed when finite elements of different dimensions are combined in the same model. Therefore, it is generally simpler and more numerically efficient than the FE/CV method.

Kang and Lee (1999) studied the process of mold filling during resin-transfer molding numerically using a modified control volume finite-element (CVFEM) method along with fixed-grid method to handle problems associated with the moving resin front. The fixed grid was refined in an adaptive manner, by dividing the flow-front elements into two regions using the estimated flow front. Imaginary new nodes were placed at the intersections between the original element border and the temporary flow front. By using the mass conservation of resin, the pressure at these newly added 'imaginary' nodes were expressed in terms of the pressure at the old 'real' nodes. Through this elimination, the imaginary nodes do not affect the size of the global matrices thus do not increase the computational time. The proposed method, namely FINE, yielded smoother flow fronts and reduced the error in the pressure at the flow front that plagued the conventional fixed-grid methods.

Shen (1998) has studied moving boundary problems of injection molding. An enthalpy model is used to predict the solid-liquid interface of the two-phase problem. An average

acceleration algorithm is developed to predict the flow front with the assumption of the average acceleration and updated boundary are corrected to meet the required volume flow rate in each time step.

2.4 Summary

Various flow models and front tracking algorithms for mold has been presented in this chapter. The application of Finite Element Method in Hele-Shaw approximation has been extensively used by many authors to solve the field problem of mold filling. The use of Hele-Shaw model in commercial package like C-MOLD and FLUENT has been reported in the literature as well. Various factors which can adversely affect the reliability and performance of encapsulated packages during filling stage like voiding, incomplete encapsulation etc. have been discussed. Experimental data from short shot in transfer molding process was used by several authors to validate their simulation results. Although many model for curing kinetics and rheology of polymeric flow reported in the literature, it was found that one cannot use the available model for verification purposes without knowing all the coefficients and curve fitting parameters derived empirically. Finally, Volume of Fluid (VOF) method and Finite Element/ Control Volume (FE/ CV) method are two most popular front tracking methods employed in the literature due to their simplicity and only one fixed mesh is required initially to simulate the advancement of fluids (Newtonian and Non-Newtonian) in mold filling problems.

Chapter 3

APPROACH FOR FLOW ANALYSIS

The present work adopted two different flow models to represent fluid flow (Newtonian or Non-Newtonian) in transfer molding. Hele-Shaw approximation has been used to study the filling phase of a transfer molding process. The field variables (pressure and velocity) obtained are input to a front tracking algorithm, namely Pseudo-concentration approach to simulate the advancement of fluid in both processes. Finite Element Method is employed in all the analyses to reduce the governing differential equations to algebraic equations.

3.1 Two-dimensional Hele-Shaw approximation

The filling phase of transfer molding can be characterized by a time-dependent, non-isothermal and non-Newtonian flow with moving free surface. Simplifying assumptions are adopted at the outset in order to solve such a formidable problem, especially in view of the geometrical complexity of common industrial components. These assumptions reduce the computational time considerably; moreover, most of the effects suppressed by these simplifications have minor consequences upon flow behavior during the filling stage. The assumptions for the present Hele-Shaw approach are as follows:

- Viscous effect dominates the flow, thus inertia effect is negligible.
- The mold is thin as compared to its length and width.
- It is an isothermal process.
- Fountain flow effect is neglected.

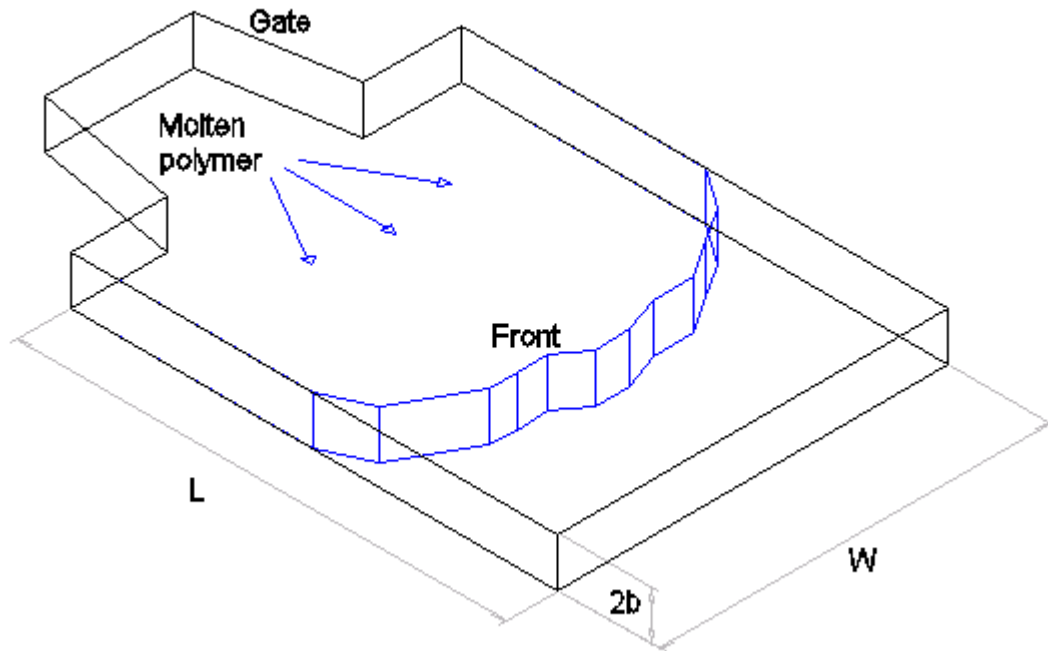


Figure 3.1: The flow of polymer melt into a thin rectangular mold cavity.

The flow of polymer melt into a thin rectangular mold cavity is depicted in figure 3.1.

The following differential equations describe the fluid flow in the cavity.

At first, the momentum equations are:

$$\frac{\partial}{\partial z} \left(\eta \frac{\partial u}{\partial z} \right) - \frac{\partial P}{\partial x} = 0 \quad (3.1)$$

$$\frac{\partial}{\partial z} \left(\eta \frac{\partial v}{\partial z} \right) - \frac{\partial P}{\partial y} = 0 \quad (3.2)$$

$$\frac{\partial P}{\partial z} = 0 \quad (3.3)$$

where η is viscosity of fluid represented by

$$\eta = \eta(\gamma)$$

and shear rate, γ is defined as

$$\gamma = \sqrt{\left(\frac{\partial u}{\partial z}\right)^2 + \left(\frac{\partial v}{\partial z}\right)^2} \quad (3.4)$$

The continuity equation is

$$\frac{\partial u}{\partial x} + \frac{\partial v}{\partial y} = 0 \quad \text{or} \quad \frac{\partial}{\partial x}(bu) + \frac{\partial}{\partial x}(bv) = 0 \quad (3.5)$$

where b is one half of the domain thickness.

Boundary conditions imposed into the system are

$$\text{At } z = \pm b, u = v = 0$$

$$\text{At } z = 0, \frac{\partial u}{\partial z} = \frac{\partial v}{\partial z} = 0$$

$$\text{At } x = L, P = 0$$

Where $z = 0$ lies in the mid-plane of the cavity.

As P does not vary in z direction, equation 3.1 can be integrated to give

$$\eta \left(\frac{\partial u}{\partial z}\right) = \left(\frac{\partial P}{\partial x}\right) z \quad (3.6)$$

$$\eta \left(\frac{\partial v}{\partial z}\right) = \left(\frac{\partial P}{\partial y}\right) z \quad (3.7)$$

Integrating equations 3.6 and 3.7 yields

$$u = \left(\frac{\partial P}{\partial x}\right) \int_z^b \frac{z \partial z}{\eta} \quad (3.8)$$

$$v = \left(\frac{\partial P}{\partial y} \right) \int_z^b \frac{z \partial z}{\eta} \quad (3.9)$$

The gap wise average velocities are obtained by integrating equations 3.8 and 3.9.

$$\bar{u} = \left(-\frac{\partial P}{\partial x} \right) \frac{S}{b} \quad (3.10)$$

$$\bar{v} = \left(-\frac{\partial P}{\partial y} \right) \frac{S}{b} \quad (3.11)$$

where fluidity, S is defined as

$$S = \int_0^b \frac{z^{\frac{n+1}{n}}}{\eta} dz \quad (3.12)$$

η is viscosity of fluid and n is power law index.

Substituting equations 3.10 and 3.11 into equation 3.5 give the flow governing equation

$$\frac{\partial}{\partial x} \left(S \frac{\partial P}{\partial x} \right) + \frac{\partial}{\partial y} \left(S \frac{\partial P}{\partial y} \right) = 0 \quad (3.13)$$

For a Newtonian fluid, shear stress varies linearly with shear rate (i.e. n = 1), thus fluidity, S becomes

$$S = \frac{b^3}{3\eta} \quad (3.14)$$

However for polymer flow, the pressure equation 3.14 becomes non-linear as fluidity is dependent on pressure gradient.

From equation 3.4, 3.6 and 3.7, it can be shown that

$$\frac{\partial U}{\partial z} = \frac{z}{\eta} \frac{\partial P}{\partial x} \quad (3.15)$$

$$\frac{\partial V}{\partial z} = \frac{z}{\eta} \frac{\partial P}{\partial y} \quad (3.16)$$

Therefore

$$\gamma = \frac{z}{\eta} \sqrt{\left(\frac{\partial P}{\partial x}\right)^2 + \left(\frac{\partial P}{\partial y}\right)^2} \quad (3.17)$$

It can be concluded that when the fluid is generalized Newtonian, equation 3.13 is a non-linear partial differential equation for pressure. An interesting simplification occurs in the case of power-law fluid for which $\eta = m_o g(T) \gamma^{n-1}$ where n is the power law index. It is then easy to show on the basis of equation 3.12 and 3.17 that

$$S = \frac{1}{A} \left(\frac{A}{m_o}\right)^{\frac{1}{n}} \int_0^b \frac{z^{\frac{n+1}{n}}}{g(T)^{1/n}} dz \quad (3.18)$$

where $A = \sqrt{\left(\frac{\partial P}{\partial x}\right)^2 + \left(\frac{\partial P}{\partial y}\right)^2}$, m_o is the material constant and $g(T)$ is a temperature function.

Nguyen (2000) concluded that transfer molding is more accurately approximated as an isothermal process because at normal and high fill rate, there is insufficient time for the resin conversion due to temperature variation to greatly affect the viscosity of the commercial transfer molding compound. Liu (2000) also is in agreement with the assumption of isothermal flow reasonably for the injection stage of resin transfer molding process as the resin is usually injected fairly fast and the filling time is much less than the curing time. Thus for isothermal process, $g(T) = 1$ and equation 3.18 reduces to

$$S = \frac{1}{A} \left(\frac{A}{m_o}\right)^{\frac{1}{n}} \left[\frac{n}{2n+1} (b)^{\frac{2n+1}{n}} \right] \quad (3.19)$$

3.1.1 Finite element formulation

Finite Element Method based on Galerkin's weighted residual approach is used to solve the flow governing partial FEM differential equation derived from Hele-Shaw approximation. The computational domain is divided into a number of small triangular elements with linear interpolation. A typical triangular element is shown in figure 3.2.

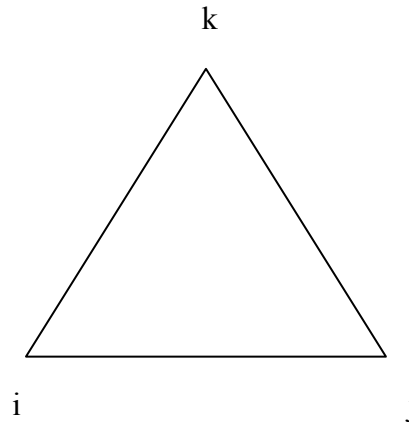


Figure 3.2: A linear three-noded triangular element

The different variables of the problem can be expressed within any triangle as:

$$P = N_i P_i + N_j P_j + N_k P_k \quad (3.20)$$

Where N_i , N_j and N_k are the shape functions for the linear triangular within any triangular element.

$$N_\beta = \frac{1}{2A} (a_\beta + b_\beta x + c_\beta y), \quad \beta = i, j, k$$

where

$$a_i = x_j y_k - x_k y_j; \quad a_j = x_k y_i - x_i y_k; \quad a_k = x_i y_j - x_j y_i;$$

$$b_i = y_j - y_k; \quad b_j = y_k - y_i; \quad b_k = y_i - y_j;$$

$$c_i = x_k - x_j;$$

$$c_j = x_i - x_k;$$

$$c_k = x_j - x_i;$$

and A is the area of the element represented by

$$A = \frac{1}{2} \begin{vmatrix} 1 & x_i & y_i \\ 1 & x_j & y_j \\ 1 & x_k & y_k \end{vmatrix}$$

3.1.1.1 Discretization of pressure equation

Galerkin's weighted residue method applied to pressure equation 3.13 gives

$$\int_{\Omega} [N]^T \left(\frac{\partial}{\partial x} \left(S_x \frac{\partial P}{\partial x} \right) + \frac{\partial}{\partial y} \left(S_y \frac{\partial P}{\partial y} \right) \right) d\Omega = 0 \quad (3.21)$$

The domain is two-dimensional with a constant thickness assigned, thus

$$\int_{\Omega} [N]^T \left(\frac{\partial}{\partial x} \left(S_x \frac{\partial P}{\partial x} \right) + \frac{\partial}{\partial y} \left(S_y \frac{\partial P}{\partial y} \right) \right) t \cdot dA = 0 \quad (3.22)$$

Where t is thickness of the domain.

The second derivative terms in equation 3.23 can be replaced by applying the product rule for differentiation. (segerland, 1984). Consider the quantity

$$\frac{\partial}{\partial x} \left([N]^T S_x \frac{\partial P}{\partial x} \right)$$

Differentiation gives

$$\frac{\partial}{\partial x} \left([N]^T S_x \frac{\partial P}{\partial x} \right) = [N]^T S_x \frac{\partial^2 P}{\partial x^2} + \frac{\partial [N]^T S_x}{\partial x} \frac{\partial P}{\partial x}$$

Rearranging and substituting for $[N]^T S_x (\partial^2 P / \partial x^2)$ term in equation 3.22

$$\int_A [N]^T S_x \frac{\partial^2 P}{\partial x^2} t.dA = \int_A S_x \frac{\partial}{\partial x} \left[[N]^T \frac{\partial P}{\partial x} \right] t.dA - \int_A S_x \frac{\partial [N]^T}{\partial x} \frac{\partial P}{\partial x} t.dA \quad (3.23)$$

Similarly for $[N]^T S_y (\partial^2 P / \partial y^2)$ term,

$$\int_A [N]^T S_y \frac{\partial^2 P}{\partial y^2} t.dA = \int_A S_y \frac{\partial}{\partial y} \left[[N]^T \frac{\partial P}{\partial y} \right] t.dA - \int_A S_y \frac{\partial [N]^T}{\partial y} \frac{\partial P}{\partial y} t.dA \quad (3.24)$$

The first integral on the right-hand side of equations 3.23 and 3.24 can be replaced by an integral around the boundary using Green's theorem.(Kreyzig, 1999). Assuming $S_x = S_y$, application of the theorem yields

$$\begin{aligned} \int_A [N]^T \left(\frac{\partial}{\partial x} \left(S_x \frac{\partial P}{\partial x} \right) + \frac{\partial}{\partial y} \left(S_y \frac{\partial P}{\partial y} \right) \right) t.dA &= \oint S [N]^T \left(\frac{\partial P}{\partial x} + \frac{\partial P}{\partial y} \right) t.dl - S \int \left(\frac{\partial [N]^T}{\partial x} \frac{\partial P}{\partial x} + \frac{\partial [N]^T}{\partial y} \frac{\partial P}{\partial y} \right) t.dxdy \\ \int_A [N]^T \left(\frac{\partial}{\partial x} \left(S \frac{\partial P}{\partial x} \right) + \frac{\partial}{\partial y} \left(S \frac{\partial P}{\partial y} \right) \right) t.dA &= \int_c N_i \left(S \frac{\partial P}{\partial x} l + S \frac{\partial P}{\partial y} m \right) t.dc - \int \int \left(S \frac{\partial P}{\partial x} \frac{\partial N_i}{\partial x} + S \frac{\partial P}{\partial y} \frac{\partial N_i}{\partial y} \right) t.dxdy \end{aligned} \quad (3.25)$$

Substituting $\bar{u} = \left(-\frac{\partial P}{\partial x} \right) \frac{S}{b}$ & $\bar{v} = \left(-\frac{\partial P}{\partial y} \right) \frac{S}{b}$ into equation 3.25 give

$$\int_A [N]^T \left(\frac{\partial}{\partial y} \left(S \frac{\partial P}{\partial x} \right) + \left(S \frac{\partial P}{\partial y} \right) \right) t.dA = \int_c N_i \left[-b \bar{u} t l - b \bar{v} t m \right] dc - \int \int \left[S \frac{\partial P}{\partial x} \frac{\partial N_i}{\partial x} + S \frac{\partial P}{\partial y} \frac{\partial N_i}{\partial y} \right] t.dxdy = 0 \quad (3.26)$$

In a simplified form, the equation 3.26 can be written as

$$[K]\{P\} = \{f\} \quad (3.27)$$

The element stiffness matrix is represented by

$$[K] = \int \int \left[S \frac{\partial N_i}{\partial x} \frac{\partial N_j}{\partial x} + S \frac{\partial N_i}{\partial y} \frac{\partial N_j}{\partial y} \right] dxdy = \int_A [B]^T [D][B] t.dA \quad (3.28)$$

where for linear triangular element,

$$\text{gradient matrix, } [B] = \frac{1}{2A} \begin{bmatrix} b_i & b_j & b_k \\ c_i & c_j & c_k \end{bmatrix} \quad (3.29)$$

$$\text{and material property matrix, } [D] = \begin{bmatrix} S & 0 \\ 0 & S \end{bmatrix} \quad (3.30)$$

Simplifying equation 3.29 gives

$$[K] = \frac{st}{4A} \left\{ \begin{bmatrix} b_i^2 & b_i b_j & b_i b_k \\ b_i b_j & b_j^2 & b_j b_k \\ b_i b_k & b_j b_k & b_k^2 \end{bmatrix} + \begin{bmatrix} c_i^2 & c_i c_j & c_i c_k \\ c_i c_j & c_j^2 & c_j c_k \\ c_i c_k & c_j c_k & c_k^2 \end{bmatrix} \right\} \quad (3.31)$$

The element forcing vector is represented by

$$\{f\} = \int_c Ni \left[-b \bar{u} t l - b \bar{v} t m \right] dc = -\frac{\bar{b} \bar{u} t l}{2} \begin{Bmatrix} N_i \\ N_j \\ N_k \end{Bmatrix} - \frac{\bar{b} \bar{v} t l}{2} \begin{Bmatrix} N_i \\ N_j \\ N_k \end{Bmatrix} \quad (3.32)$$

where t is the element thickness and l is element length subjected to boundary condition.

Thus, element equation represents the flow can be written as

$$[K]^e \{P\} = \{f\}^e$$

$$[K] = \frac{st}{4A} \left\{ \begin{bmatrix} b_i^2 & b_i b_j & b_i b_k \\ b_i b_j & b_j^2 & b_j b_k \\ b_i b_k & b_j b_k & b_k^2 \end{bmatrix} + \begin{bmatrix} c_i^2 & c_i c_j & c_i c_k \\ c_i c_j & c_j^2 & c_j c_k \\ c_i c_k & c_j c_k & c_k^2 \end{bmatrix} \right\} \begin{Bmatrix} P_i \\ P_j \\ P_k \end{Bmatrix} = -\frac{\bar{b} \bar{u} t l}{2} \begin{Bmatrix} N_i \\ N_j \\ N_k \end{Bmatrix} - \frac{\bar{b} \bar{v} t l}{2} \begin{Bmatrix} N_i \\ N_j \\ N_k \end{Bmatrix} \quad (3.33)$$

For Newtonian fluid, $S = \frac{b^3}{3\eta}$ which is a linear problem

For isothermal non-Newtonian fluid, $S = \frac{1}{A} \left(\frac{A}{m_o} \right)^{\frac{1}{n}} \int_0^b z^{\frac{n+1}{n}} dz$

where $A = \sqrt{\left(\frac{\partial P}{\partial x} \right)^2 + \left(\frac{\partial P}{\partial y} \right)^2}$